Development of a Shipboard Lidar: Technical Layout and First Results

R. Reuter and R. Willkomm

Carl von Ossietzky University, Physics Department, P.O.Box 2503,
D-26111 Oldenburg, Germany

G. Krause and K. Ohm

Alfred Wegener Institute for Polar and Marine Research,
Section Marine Physics, D-27568 Bremerhaven, Germany

ABSTRACT

Fluorescence spectra of seawater include information on several substances like gelbstoff, chlorophyll, aromatic molecules and particles. Vertical profiles of their concentration in the water column can be derived from a time-resolved registration of laser induced fluorescence, water Raman and elastic (Mie) scattering. First test measurements of this kind were performed in the Atlantic Ocean with a newly developed hydrographic lidar installed on board of RV "Polarstern". Series of depth profiles were obtained along the ship track with a vertical resolution of 0.5 m, typically, in water having an optical attenuation coefficient of about 0.2 m^{-1}. Penetration depths ranged up to 40 m, depending on the seawater turbidity.

INTRODUCTION

Visible light is the only portion of the electromagnetic spectrum which can be transmitted through water. Therefore, lidar remote sensing allows an evaluation of water column parameters with instruments either installed on board a ship (Dudelzak et al., 1991; Cecchi et al., 1992; Babichenko et al., 1994; and others) or an aircraft (Hoge and Swift, 1982; Bristow et al., 1985; Reuter et al., 1993; and others). Compared to optical radiometers which measure the sunlight-induced water leaving radiance spectrum, lidar generally makes use of pulsed lasers and is therefore independent of daylight. Moreover, the monochromatic excitation of many organic substances and the specific detection of their fluorescence emission leads to a high information content of lidar data particularly in coastal waters (Schmitz-Peiffer et al., 1990a,b).

Hydrographic measurements with lasers are mostly performed in a fluorosensing mode, where an integration of the returned signal is done. Only a few attempts have been made to gather laser-induced data in a time-resolving detection mode, thus making use of the short laser pulse to probe the fluorescence decay time of a target, or to measure the depth distribution of fluorescent or scattering material.

The fluorescence decay time of oils floating on the sea surface has been shown to be a very specific parameter which allows to classify oils better than using the fluorescence intensity spectrum (Measures, 1984; Diebel et al., 1987b; Camagni et al., 1991; and others). This has led to the development of an airborne lidar with high spectral and temporal resolution capabilities for oil spill detection (Verdebout and Koechler, 1992).

A first approach to measure water column parameters with time-resolving lidar aimed at the evaluation of seawater temperature profiles from the measured spectral shape of the water Raman scattering peak (Leonard et al., 1979). Other applications were the estimation of attenuation profiles from elastic particle backscattering (Hoge et al., 1988) which were also measured with bathymetric (i.e. water depth sounding) lidars (Phillips, 1981; Billard et al., 1986).

Only a few efforts have been made to use airborne lidars for measuring time-resolved signals of water Raman scattering (Hoge and Swift, 1983) and fluorescence with the objective of extracting depth profiles of attenuation coefficients and fluorescent matter concentrations in the upper water column (Diebel-Langohr et al., 1986). It could be shown that an optical penetration depth of about 6 attenuation lengths can be obtained, which corresponds to about 15 m water depth in the Adriatic and the southern North Sea in these experiments (Diebel, 1987a).

To achieve such depth profiles it was necessary to confine the lidar measurements to night-time, since the daylight induced background severely degrades the weak signal intensities from deeper water layers. Secondly, an average over several hundreds of shots was necessary to increase the signal-to-noise ratio to a level which was sufficient for extracting a stable time-resolved signal return. Therefore

only a relatively low resolution has been achieved, with depth profiles averaged over distances of about 1 km along the flight line of the aircraft.

However, the results of measuring depth-resolved data of hydrographic parameters with an airborne fluorescence lidar were so encouraging that a further development of this method was envisaged. The above-mentioned limitations of the sunlight-induced background which interferes with the time-resolved lidar return, and the necessity of averaging these signals over many single shots were considered less critical in case of shipboard applications due to the in-water shadow produced by the ship itself, and because of its lower speed. Furthermore, operation on board a research vessel would allow to make use of a lidar over extended periods of time, which is of particular value within long-term monitoring programmes.

It was therefore decided to design and to build a new instrument within the Eureka Programme EUROMAR, for operation on board the research vessel "Polarstern" of the Alfred-Wegener-Institute for Polar and Marine Research, Bremerhaven. Due to the extensive campaigns of this ship to polar regions, this opens a way to gather remotely sensed profiles from the upper water layers over large areas of the open oceans, while the ship is underway and without any restriction to its operation (velocity, manoeuvring). Also, the regular transects in the Atlantic Ocean between Europe and the Antarctic offer unique possibilities to employ a shipborne lidar on this vessel.

Although identical in principle, air- and shipborne lidars face different problems in practice. If carried by an aircraft some hundreds of metres above the sea surface the time elapsed between sending out the laser pulse and the return of the signal from the water column is about 1 microsecond. This is sufficient to avoid electromagnetic interference from the laser power electronics to the sensitive detectors and signal amplifiers. This is not the case for a lidar system on board of a ship where signals have to be registered within a few nanoseconds following the laser pulse emission, and it is a great challenge to avoid noise due to electromagnetic interference in the near-field of operation.

1. DESIGN OF THE INSTRUMENT

1.1. General considerations

A major goal of the lidar development was to realize a prototype with a modular concept of interchangeable optical and electronic components, thus allowing a flexible configuration of this instrument type for different tasks in future. This requirement can be easily fulfilled for the laser and detector subsystems. However, two methods of integrating the lidar into the ship were possible with different consequences for the flexibility of its use on board other ships:

- an autonomous layout of the instrument for a stand-alone operation in a ship's laboratory, with a near-nadir field of view towards the sea surface by use of optical mirrors.

This solution was not considered further. First, the advantage of having a reduced daylight intensity in the region of the shadow of the ship and hence a lower background signal would have been lost, and secondly, the transmission through the rough sea surface has a strong and variable influence on the raypath of the laser pulse and the detector field of view.

- a rigid integration into the hull of the ship, with a path of rays leading through an optical window (Fig. 1).

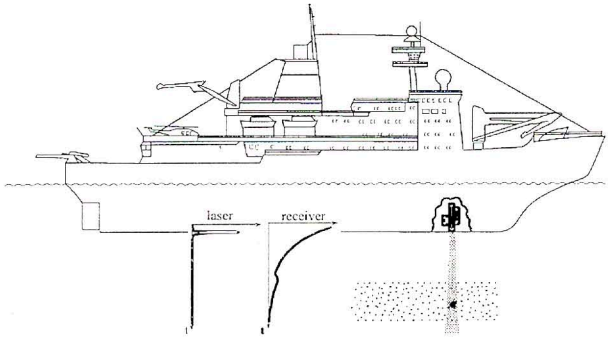

Fig. 1 - Installation of the lidar on board the RV "Polarstern", in the shadow of the hull at 11 m depth below the sea surface.

Although an easy installation on board other vessels would be very difficult or even impossible, this method was chosen because it offers the most efficient suppression of daylight and a well-defined optical interface between the water column and the instrument. However, the lidar as an integral part of the ship's hull led to constraints for the layout of the mechanical structure, since the safety requirements for installing a glass window near the keel have to be met.

These considerations resulted in a mechanical structure of the lidar with the telescope as the central element to which the laser and the detector unit are rigidly coupled to maintain a stable optical alignment (Fig. 2). The telescope is closed towards the water column by a quartz window. The telescope housing is pressure proved, with a tube. thickness which corresponds with that of the ship's hull. To achieve a coaxial structure of the laser beam axis and telescope field of view, both the laser light and the telescope output pass through small windows at the side of the telescope housing which are automatically closed in case of water intrusion into the telescope.

Time-resolved data of elastic backscattering, water Raman scattering, and of gelbstoff fluorescence (Fig. 3) are derived in a spectral region where the transparency of seawater is

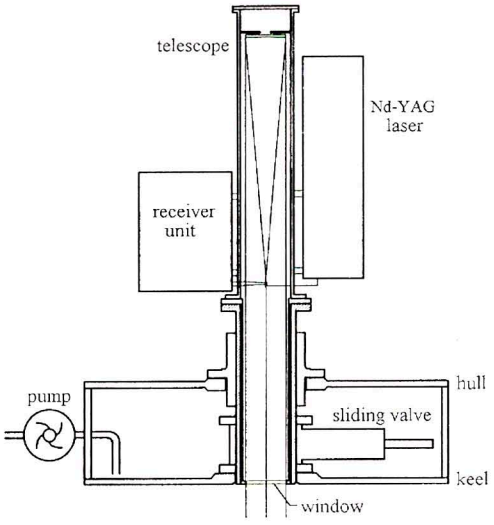

Fig. 2 - Schema of the lidar installed near the keel of the ship. The mechanical construction allows the installation of the system including the window without docking of the ship. To remove the lidar, the whole telescope setup is lifted, and then the sliding valve is closed. Together with the gasket in the hull it forms a sluice which maintains the ship's security.

high, with laser pulses having a pulse length of about 1 nanosecond. The frequency-doubled (532 nm) and tripled (355 nm) output of a Nd:YAG laser provides emission wavelengths which are suitable in coastal regions with a transparency maximum at green wavelengths, and in clear oceanic waters. An optical penetration depth of more than four attenuation lengths was anticipated in these spectral regions, which corresponds to water depths of 10 to 20 m in coastal areas, and more than 40 m in clear oceanic conditions, depending on the transparency of water.

Other fluorescence signals (Fig. 3) which are outside the blue-green optical window can be detected, but because of the high attenuation the penetration depth is so small that time resolution is not applicable there. The 685 nm fluorescence of chlorophyll a e.g. can be measured from the upper few metres of the water column only (Poole and Esaias, 1982; Venable et al., 1984). This holds also with the near-UV fluorescence of aromatic amino acids, like tryptophan, which are fluorescent constituents of algae and bacteria (Determann et al., 1994). A fluorescence excitation of these aromatic amino acids requires an excitation wavelength in the 230 or 270 nm range (Tatischeff and Klein, 1976).

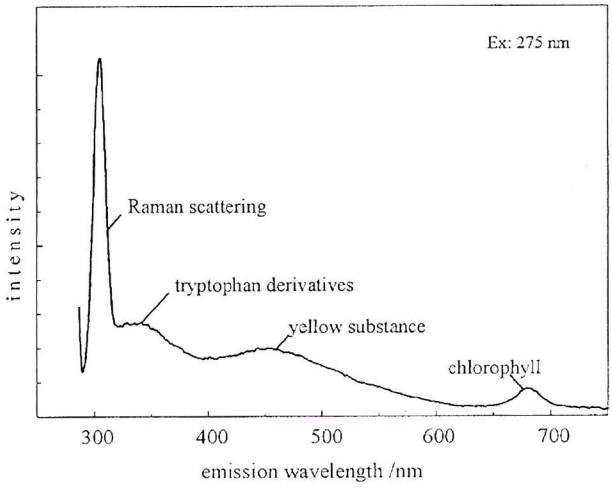

Fig. 3 - Typical fluorescence emission spectrum of seawater, showing Raman scattered light and fluorescence signatures of different substances.

1.2. Laser

An active-active mode-locked Nd:YAG laser system model SYL A2 from Quanta Systems is used. Short pulses of about 1 ns are generated by Q-switching and a superimposed harmonic modulation of the quality of the resonator. With harmonic generation and a N_2 Raman shifter applied to the fourth harmonic of the Nd:YAG fundamental, a set of three wavelengths in different spectral regions is obtained which can be used to specifically excite fluorescent substances, and to provide a maximum penetration depth in turbid coastal and clear oceanic waters (Table 1).

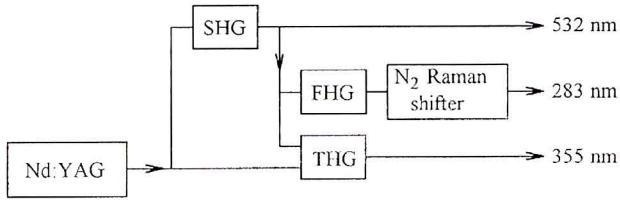

Fig. 4 - Generation of different excitation wavelength from the fundamental line of the Nd:YAG at 1064 nm.

1.3. Telescope

Light from the water column is received by an f/6 Newtonian telescope with a 20 cm entrance aperture. The field of view is limited by a diaphragm with 3 mm diameter fixed on the surface of a prism which is used as a secondary folding mirror for deflecting the light from the primary mirror to the detectors outside the telescope tube.

Due to the position of the diaphragm close to the focus of the primary mirror, the near-field sensitivity of the telescope is strongly reduced. This is a desired effect, resulting in much lower requirements for the dynamic range of the detector electronics when compared to a $(1/\text{distance})^2$ sensitivity dependence (Fig. 5). Further details of the telescope optics are given in another paper in this volume (Ohm and Willkomm, 1994).

Table 1: The Laser.

type:		**Nd:YAG with Q switching**	
wavelengths:		**used for excitation of:**	
532 nm	(2nd harmonic)	532 nm	elastic scatter
		650 nm	water Raman
		685 nm	chlorophyll a flu. excited via fucoxanthin
355 nm	(3rd harmonic)	355 nm	elastic scatter
		405 nm	water Raman
		430 nm	gelbstoff flu.
283 nm	(4th harmonic, N2 Raman shifted)	313 nm	water Raman
		344 nm	tryptophan flu

output characteristics

wavelengths	532	355	283	nm
energy	50	25	3	mJ
beam divergence	0.4	0.3	0.5	mrad

pulse length	< 1 ns
repetition rate	10 Hz max

1.4. Detectors

The incident beam of light is split into different wavelength bands by dichroic mirrors. Great care was taken to the problem of achieving identical optical conditions for every detector, in particular to an identical illumination of their photocathodes within the range of penetration depths into the water column. Also, the distances between telescope output aperture and photodetectors, and hence the time elapsed between laser firing and signal recovery at each detector, have to be identical, since the output signals of different channels need to be combined to calculate the depth profile of fluorescent substances, e.g. the fluorescence and water Raman channels.

This is achieved by an arrangement of detectors in a binary tree structure, with dichroic beamsplitters used for separating different spectral ranges, which results in equivalent optical paths for each detector (Fig. 6). The detector unit consists of four detection modules, each capable of carrying four detection channels as a maximum (Fig. 7). Fast compact head-on PMT are used as detectors. Their current amplification is gated by switching the voltage level of a dynode, to prevent a non-linear response due to daylight background; the gate control circuit is triggered by the laser output, with a gate-on period limited to 3 µs. In addition to the photodetector and optical filter assembly, each channel is equipped with an HV converter for PMT operation and other electronic control circuits, and is therefore autonomous. Furthermore, detection wavelengths (Table 2) can be changed in a modular way to adapt the instrument to new applications.

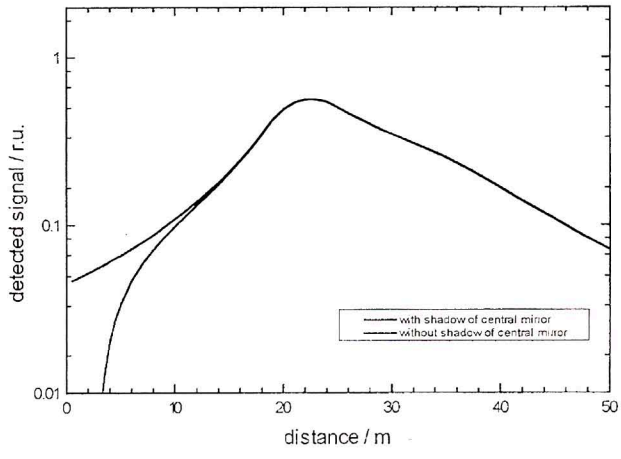

Fig. 5 - Calculated detection signal as a function of distance to the main mirror with and without secondary mirror (focal length 1.200 m, aperture f/6, distance diaphragm - main mirror 1.253 m, distance secondary mirror - main mirror 1.243 m, diaphragm 3 mm, laser divergence 0.5 mrad).

Table 2: The Receiver.

telescope:		
Type	Newtonian	
focal length	1200 mm	
f-number	f/6	
entrance aperture	20 cm	
spectrograph and detectors:		
number of channels	16 max.	
wavelength selection	binary tree of dichroic beamsplitters; interference and glass blocking filters	
	miniaturized head-on PMT	
photodetectors	UV/blue: Hamamatsu model R1893	
	green/red: Hamamatsu model R1635	
wavelengths/bandwidth:	used for detection of:	
313 / 10 nm	water Raman scatter	$\lambda_{Ex} = 283nm$
344 / 10 nm	water Raman scatter	$\lambda_{Ex} = 283nm$
405 / 10 nm	water Raman scatter	$\lambda_{Ex} = 355nm$
430 / 10 nm	gelbstoff fluorescence	
532 / 1 nm	elastic scattering	$\lambda_{Ex} = 532nm$
650 / 10 nm	water Raman scatter	$\lambda_{Ex} = 532nm$
313 / 10 nm	water Raman scatter	$\lambda_{Ex} = 283nm$
685 / 10 nm	chlorophyll a fluorescence	

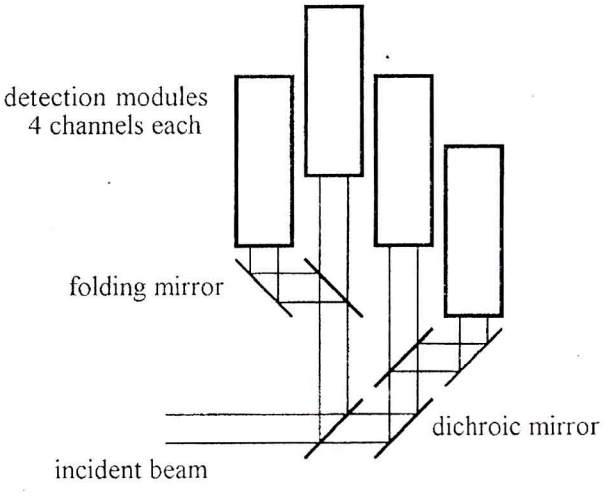

Fig. 6 - Separation of different wavelength by a binary tree of dichroic mirrors in the detection unit. Each detection module contains up to four channels. The optical length of each light path is the same.

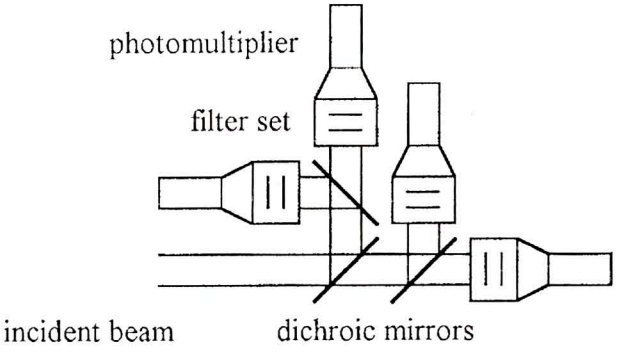

Fig. 7 - Optical module consisting of four detection channels including separation of spectral bands by dichroic mirrors and wavelength selection by interference filters.

1.5. Data acquisition

Laser-induced signal returns from the water column cover a high dynamic range due to the exponential decrease of the signal intensity versus penetration depth. In addition to the above-mentioned sensitivity reduction of the telescope in the near-field (Ohm and Willkomm, 1994), an additional dynamic compression is obtained in the data acquisition unit by use of fast logarithmic amplifiers, with an input range of nearly 4 orders of magnitude and an output signal fall time of about 5 ns per decade (Table 3).

Data sampling and digitization is performed with a Tektronix transient recorder at a rate of 1 GHz for up to four channels in single shot with a resolution of 8 bit (Table 3). In the actual state of its development the input range of signal intensities is limited by different factors: strong signals from the water column from distances close to the exit quartz window are limited by overload of photomultipliers,

Table 3: Data Acquisition.

signal recovery:			
dynamic compression	logarithmic amplifier		
	Analog Modules model 382		
	Input range -75 dB, related to 2 V @ 50 Ω		
transient digitizers	Tektronix model DSA 602 A		
acquisition channels	2	4	6
gigasamples / s	2	1	0.5
depth resolution of signal recovery/cm	6	11	23

which leads to degraded trailing edges of the signal return from deeper layers when operated in the upper range of their specified HV voltages. At low levels, signal recovery is limited by (i) electromagnetic interference from the laser, which will be reduced by a better shielding in future, and (ii) by the lower limit of dynamic range of the logarithmic amplifier. Its transfer function becomes linear with output signals of less than -40 mV, which is about 3 times higher than the daylight background at blue wavelengths. Attempts will be made to better adapt the PMT signal range to the dynamic range of the logamps, and to calibrate the logamp transfer function at low signal levels. It is expected that these improvements lead to an increase of the optical penetration depth of the instrument up to at least 6 attenuation lengths, compared to 4 attenuation lengths available in the present state of its development.

1.6. Instrument Control

A VME Bus computer is used to control the measuring process, and to store the data on magneto-optical disk. Data interpretation and visualization are actually done with a Personal Computer. However, in future the multitasking capability of the VME Bus computer will be utilized to perform the data interpretation in real time.

2. DATA INTERPRETATION

The calculation of depth profiles of attenuation coefficients and fluorescent matter concentrations from the time-resolved return signals is based on previously published papers on depth-resolving airborne lidar (Diebel-Langohr et al., 1986; Diebel, 1987a). Therefore, these algorithms are only briefly summarized here.

A lidar signal received from a layer in depth z is described by the lidar equation:

$$I(z, \lambda_D) = \int_{z''=z}^{z+\Delta z} I_{0,\lambda_L} e^{-\int_0^z c(z', \lambda_L)\, dz'} k_i(z)\, A_\rho(z)\, \eta_i \; e^{-\int_0^z c(z', \lambda_D)\, dz'} \qquad (1)$$

with λ_D detection wavelength

λ_L laser wavelength

I_{0,λ_L} energy of the laser pulse

$I(z)$ energy received from water layer of thickness Δz in depth z

$S(z)$ sensitivity of the optical setup (dimension sr)

$k_i(z)$ molecular concentration of substance i (dimension $mol \cdot m^{-3}$)

η_i molecular signal cross section of substance i (dim: $mol^{-1} \cdot sr^{-1}$)

$c(z, \lambda)$ attenuation coefficient at wavelength λ with depth.

$A_\rho(z)$ illuminated area in depth z

The sensitivity function $S(z)$ takes the beam divergence of the laser, the field of view, and the angle of receipt of the telescope into consideration. She is discussed in detail in another paper in this volume (Ohm and Willkomm, 1994). The total attenuation coefficient at a given detection and excitation wavelength can be derived if concentration and cross section of a substance are constant, as it is the case for the Raman scattered light in seawater. It follows from the analysis of the depth-resolved water Raman scatter signal $I(z, \lambda_R$ measured at the water Raman scatter wavelength λ_R:

$$c(z, \lambda_L) + c(z, \lambda_R) = \frac{1}{\Delta z}\left[ln\left(\frac{I(z, \lambda_R)}{I(z+\Delta z, \lambda_R}\right) - ln\left(\frac{S(z, \lambda_L, \lambda_R)}{S(z+\Delta z, \lambda_L, \lambda_R}\right)\right] \qquad (2)$$

Due to multiple scattering effects the attenuation coefficient derived in this way is not exactly the beam attenuation coefficient (Poole and Esaias, 1982; Gordon, 1982; Punjabi and Venable, 1986) but corresponds to some intermediate value of the beam and diffuse attenuation coefficients, depending on the scattering characteristics of the hydrosol and on the optical geometry of the lidar.

The length of the depth interval Δz which is applied to the depth-resolved signal is equivalent to the path length of conventional photometers. The dependence of this path length on the accuracy of the attenuation measurement (Austin, 1977), which is also a function of the attenuation coefficient itself, holds also with the depth interval Δz applied to the interpretation of lidar data. Resulting from the accuracy of the measured depth profiles which are obtained with the lidar in the present state of its development, the

product of attenuation coefficient c and depth resolution Δz is invariant with $c \cdot \Delta z \approx 0.1$. This means that in the case of low hydrosol concentration and hence low turbidity of the water, a high depth resolution is made impossible by the low dynamics of the returned signal, and enhanced turbidity will lead to better depth resolution but lower penetration depth.
Profiles of substance concentrations $k_i(z)$ are derived from their specific fluorescence signals and from the Raman scattered light by means of a Raman normalisation:

$$\frac{I(z, \lambda_D)}{I(z, \lambda_R)} = k_i(z) \frac{\eta_i}{k_R \eta_R} \frac{S(z, \lambda_L, \lambda_D}{S(z, \lambda_L, \lambda_R)}$$

$$e^{-\int_0^z [c(z', \lambda_D) - c(z', \lambda_R)] dz'}$$

from which it follows:

$$k_i(z) = \frac{k_w \eta_R}{\eta_i} = k_i(z) \frac{I(z, \lambda_D)}{I(z, \lambda_R)} \frac{S(z, \lambda_L, \lambda_R)}{S(z, \lambda_L, \lambda_D)}$$

$$e^{-\int_0^z [c(z', \lambda_D) - c(z', \lambda_R)] dz'}$$

with η_R Raman scattering cross section of water and k_w the concentration of water molecules.
If the sensitivities of the detection channels are the same with respect to distance as outlined in sect. 1.4, the concentration profiles can be written as:

$$k_i(z) = \alpha \frac{I(z, \lambda_D}{I(z, \lambda_R)} e^{-\int_0^z [c(z', \lambda_D) - c(z', \lambda_R)] dz'} \quad \text{with}$$

$$\alpha := \frac{k_w \eta_R}{\eta_i} \frac{S(\lambda_R)}{S(\lambda_D)}$$

The difference between the attenuation coefficients at the water Raman and the chosen fluorescence detection wavelength which has been neglected in this approximation represents a serious problem: it can give rise to systematic errors of the calculated depth profile with increasing relevance for deeper water layers (Diebel, 1987a).

3. EXPERIMENTAL RESULTS

The lidar was installed on board RV "Polarstern" for the first time in January 1993. The goal was to test the complicated mechanical structure and its integration into the hull of the ship, and to verify the optical alignment on board which had been set up in the laboratory prior to the shipboard installation. It turned out that the mechanical design fulfilled all expectations.
Secondly, time-resolved signals were to be recorded to find out whether a depth penetration of 40 m into the water column is attainable in clear oceanic waters. In practice, the evaluation of depth profiles was difficult because of serious electromagnetic interference. The source of this noise which lies in the 100 MHz range, i.e. in the centre of the frequency range of interest for these measurements, was the laser head and its electrical connection to the power supply rack.
Following these first performance tests, the second operation of the lidar aimed at the investigation of subsurface structures along the ship's track. This was done during the cruise ANT XI/1 of RV "Polarstern" between Bremerhaven, Germany, and Cape Town, South Africa. With 355 nm excitation, water Raman scattering and the fluorescence of gelbstoff and chlorophyll were measured. Elastic backscattering, water Raman scattering and chlorophyll fluorescence were measured with 532 nm excitation (Table 2). Near-surface temperature and salinity (OTS probing system of ME Meerestechnik-Elektronik, Germany), and chlorophyll fluorescence and hydrosol backscattering data (Haardt Optik-Mikroelektronik, Germany) were continuously measured using probes installed in the hydrographic well of the ship. T/S depth profiles (Seabird 911 plus CTD system) were also obtained at stations together with chlorophyll and gelbstoff fluorescence profiles by use of an *in situ* fluorometer (Haardt Optik-Mikroelektronik, Germany) which served as a reference for the lidar measurements. Moreover, water samples were taken for plankton pigment analysis with HPLC, and for measurements of fluorescence spectra with a Perkin Elmer LS50 spectrofluorometer. Ship cruise and depth stations are shown in Fig. 8.
Only part of the measurements obtained in the cruise have been evaluated so far. To give an example, the results obtained in the South Atlantic Ocean (54°45'S, 9°10' E, Fig. 8), where large horizontal gradients of the hydrographic parameters were observed, are reported in the following. Fig. 9 shows near-surface data of temperature, salinity and hydrosol backscattering measured along the ship's track. In the central part of this transect a strong gradient of hydrosol backscattering is observed which indicates a variation of suspended matter concentrations, while temperature and salinity show only small variations.
The time-resolved lidar signal of water Raman scattering with 355 nm excitation is strongly affected by the variations of the hydrosol content. Fig. 10 shows two examples of these signals which correspond to averages of 256 single shots. They demonstrate that a penetration depth of 25 and 10 m was reached in the clear and turbid waters of this region. Two problems are apparent in these curves. The intensity at the leading edge of the turbid water signal is higher when compared with the clear water signal. However, because of the constant water Raman scatter efficiency lower intensities are to be expected for the entire curve obtained in turbid waters. The observed discrepancy is probably due to elastic multiple scattering in the region of enhanced hydro-

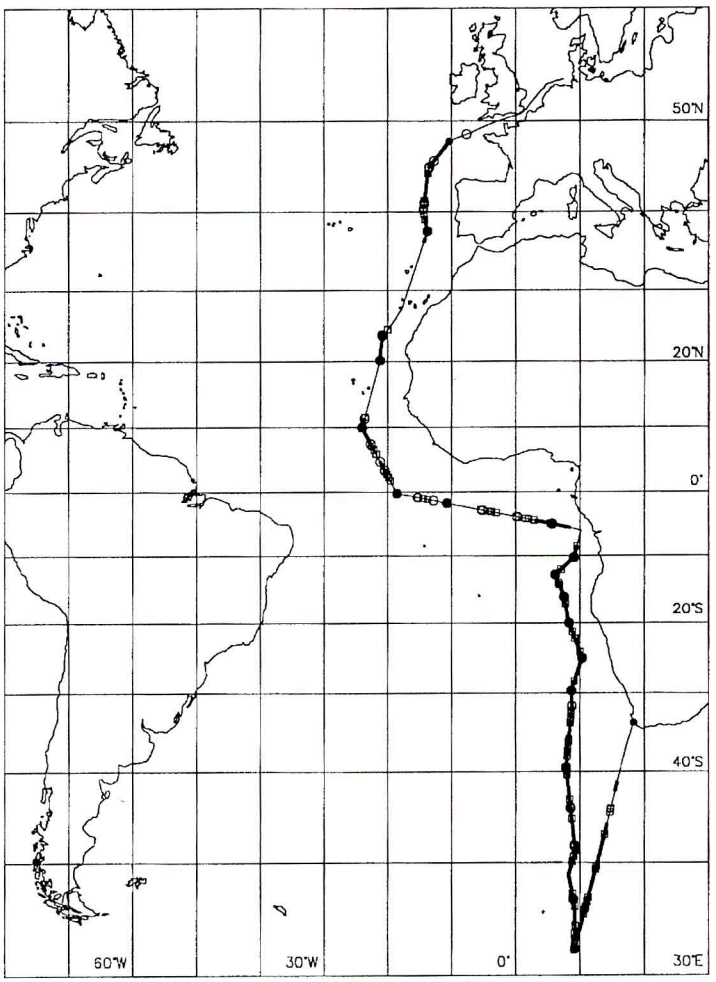

Fig. 8 - Cruise of RV "Polarstern" between Bremerhaven, Germany (October 18, 1993) and Cape Town (November 27, 1993). The lidar was operated along the cruise track shown as full line. Dots correspond to depth stations, open circles to HPLC sampling positions for plankton pigment analysis, open squares to sampling positions for in vitro fluorescence measurements.

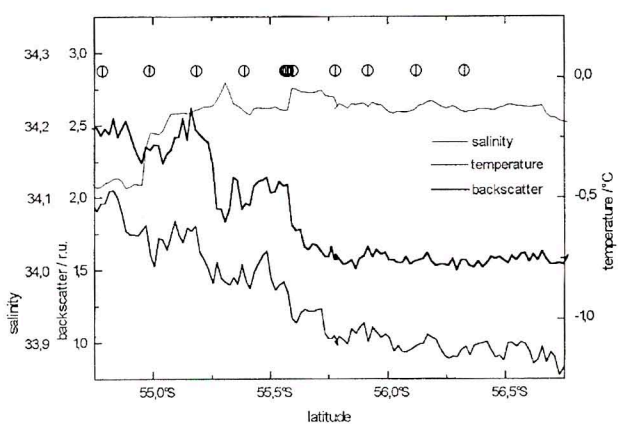

Fig. 9 - Temperature, salinity and hydrosol backscattering measured with in situ probes in the hydrographic well on 20 November 1993 south of 54°45'S, 9°10'E. Positions of lidar profiles shown in Fig. 11 are marked by symbols.

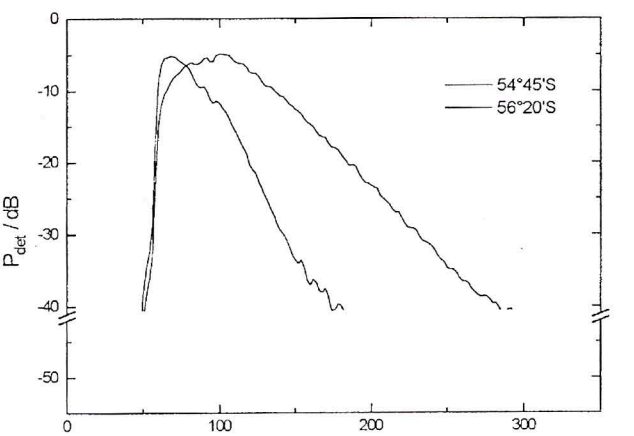

Fig. 10 - Examples of raw data of 405 nm water Raman scatter with 355 nm excitation, taken at the begin and the end of the cruise track data in Fig. 9 and the lidar depth profiles in Fig. 11. The signal with fast decay of the trailing edge corresponds to an attenuation coefficient $c(355) + c(405) = 0.4\ m^{-1}$, the signal with slower decay to $c(355) + c(405) = 0.16\ m^{-1}$.

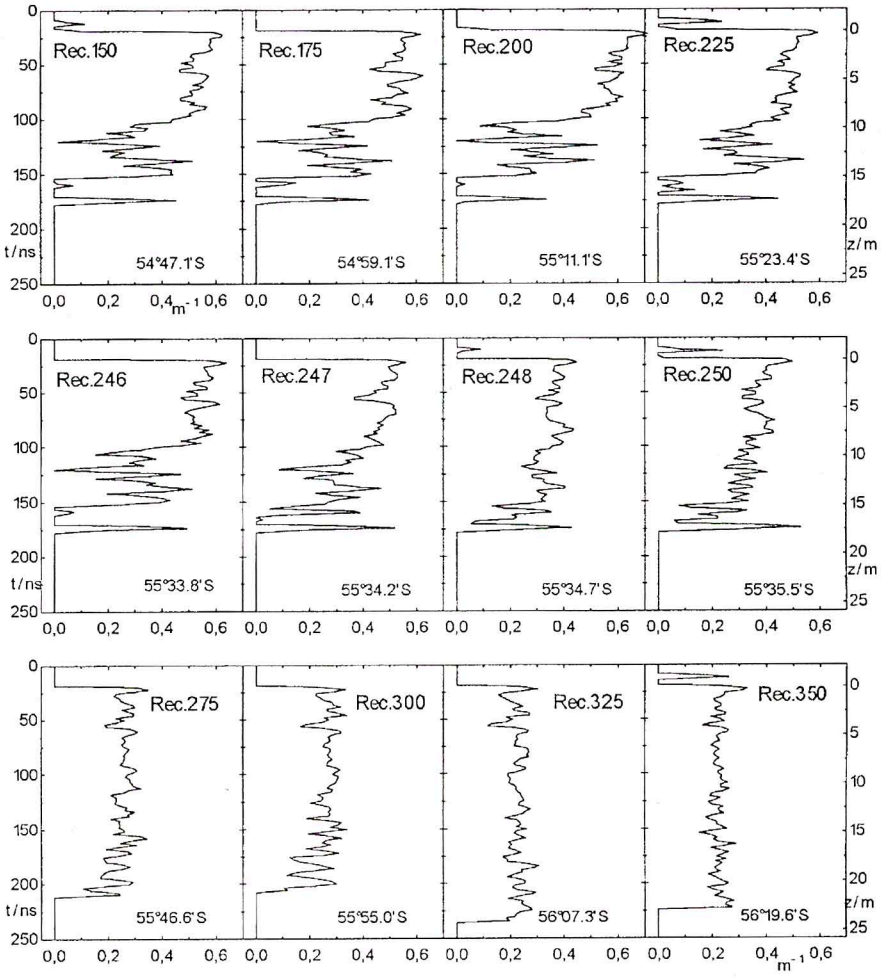

Fig. 11 - Depth profiles of the attenuation coefficient c(355) + c(405) calculated from time-resolved lidar data along the ship track shown in Fig. 9. The degradation of the upper portion of the curves is prèsumably due to multiple scattering as discussed in the text. The fine structure is caused by superimposed electromagnetic noise.

sol content, which produces straylight outside the shadow region of the telescope field of view in the near field, thus giving rise to enhanced contributions of detected water Raman scattering. Secondly, electromagnetic interference is still present in the signals, and this severely degrades the weak contributions from deeper water layers. A further improved shielding of the laser which is again the source of this interference, should lead to an increase of the penetration depth by a factor of approximately 1.5.

From these raw data, depth profiles of attenuation coefficients c(355) + c(405) (Fig. 11) have been calculated. A critical step in their evaluation is the depth-dependent sensitivity of the telescope (Ohm and Willkomm, 1994), which is described by the function S (z , λ_L , λ_R) in Equ. (1). This function depends sensitively on the optical alignment of the instrument, it needs to be determined experimentally in homogeneous water. However, S (z , λ_L , λ_R) cancels out when subtracting two depth profiles of the attenuation coefficient, Equ. (2). Fig. 12 shows for the two profiles given in

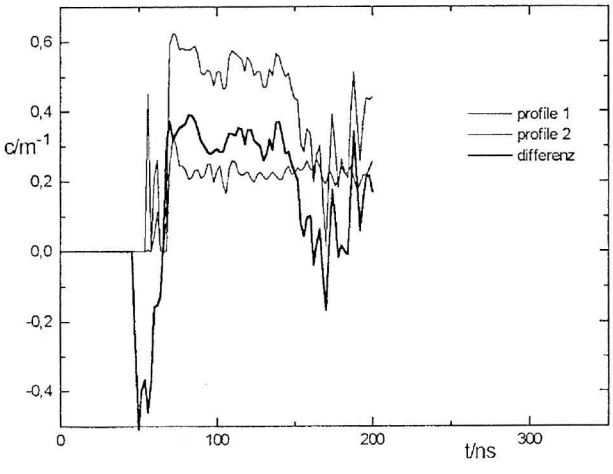

Fig. 12 - Depth profiles of the attenuation coefficient c(355) + c(405) constructed from the curves shown in Fig. 10, and their difference from which the sensitivity function S given in Equ. (1) and (2) should cancel out.

Fig. 10 that this is not the case in the near-field of the telescope. Assuming the attenuation coefficient to be relatively homogeneous near the sea surface, this supports again the hypothesis of an unstable sensitivity function S due to multiple scattering as discussed above.

Another example which displays the entire set of time-resolved signals at the various detection wavelengths and with 355 and 532 nm excitation is shown in Fig. 13. The data were registered at positions 53°30'S, 9°00'E on Nov. 19, 1993 (Fig. 9). The distribution of fluorescent matter is virtually homogeneous in the near-surface layer within the penetration depth of the lidar, as shown by the reference data in Fig. 14.

The attenuation coefficients at this position as derived from the water Raman signals are $c(355) + c(405) = 0.34\ m^{-1}$ and $c(532) + c(650) = 0.51\ m^{-1}$ in average. The 532 nm elastic scatter signal results in an attenuation coefficient of $c(532) = 0.33\ m^{-1}$. The depth from which chlorophyll fluorescence can be measured is much smaller than with the other scattering and fluorescence channels, as it is to be expected from the high absorption coefficient of the water at the chlorophyll fluorescence wavelength.

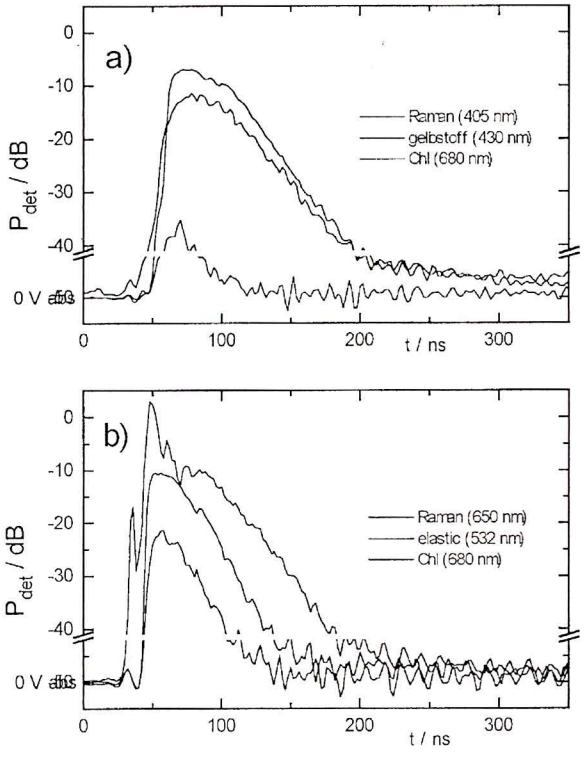

Fig. 13 - Time-resolved signals of 405 nm water Raman scatter, 430 nm gelbstoff and 680 nm chlorophyll fluorescence with 355 nm excitation (a), and of 532 nm elastic and 650 nm water Raman scatter and 680 nm chlorophyll fluorescence with 532 nm excitation (b). The peaks at 32 ns elapsed time are due to straylight from the laser beam folding prism in the optical axis of the telescope. The strong peak in the 532 nm signal at 45 ns elapsed time is due to laser light reflected at the quartz window which separates the instrument from the water column.

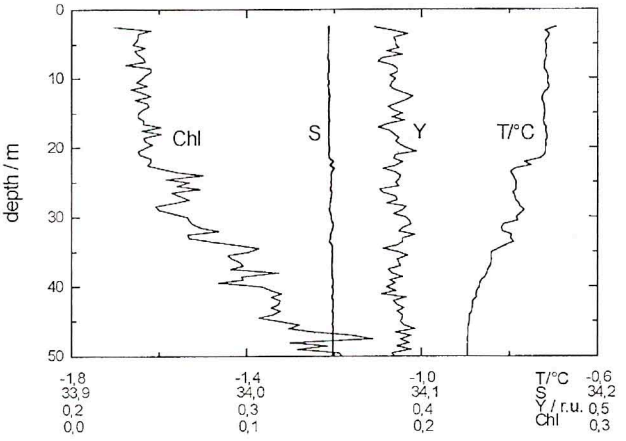

Fig. 14 - Depth profile of temperature, salinity, and of chlorophyll and gelbstoff fluorescence measured in parallel to the lidar signals shown in Fig. 13.

CONCLUSION

It has been the aim of the development of the shipboard hydrographic lidar to provide a new type of instrument for the following purposes:

- to derive a maximum of remotely sensed information on optical properties from the upper water column as can be obtained from board of a moving ship without limitations on its velocity.
- to provide data on hydrosols, phytoplankton, on dissolved organic substances (gelbstoff) and other fluorescent materials like hydrocarbons or tracer dyes which are relevant to biological and chemical studies in the open ocean and in coastal waters.

The high expenses required during the prototype development for its installation as part of the ship hull will be of minor importance if research vessels built in the future are equipped with appropriate installations, as they are required for other instruments as well, e.g. acoustic doppler current profilers.

In its actual state of development, the prototype of the shipboard lidar has demonstrated that depth resolved profiles of optical properties of seawater can be measured in the near-field and down to acceptable depths. However, the lidar will need some further refinements:

- the dynamic range of signal recovery from the water column has to be improved, e.g. with a better electromagnetic shielding of the sensitive detection system
- size and weight of the instrument should be reduced for a better handling on board of a ship
- the data interpretation has to be done in real time to support the research of marine biologists and chemists by providing them with continuous and actual information on the horizontal and vertical distribution of matter in the water column.

ACKNOWLEDGEMENTS

This work is financially supported by the Federal Minister of Research and Technology, Bonn, within the frame of Euromar. The support of the Hapag Lloyd Werft, Bremerhaven, and of the electronics and mechanics workshop of the University of Oldenburg during the development of the mechanical and electronic structure of the lidar are particularly acknowledged. We are also indebted to the electronics engineer O. N nberg and the technician K. Loquay from the Remote Sensing Working Group at the University of Oldenburg. The authors wish to extend their personal thanks to the captain and the crew of RV "Polarstern" for their support during the experiments on board the ship.

REFERENCES

Austin, R.W., 1977, Precision considerations in the measurement of volume attenuation coefficients. In: Tyler, J.E. (editor), Light in the Sea. Dowden, Hutchinson & Ross, Stroudsburg, Pennsylvania, p. 121-124

Babichenko, S., Kaitala, S., and Poryvkina, L., 1994, Multiple-wavelength remote sensing of phytoplankton. EARSeL Advances in Remote Sensing, published in this volume.

Billard, B., Abbot, R.H., and Penny, M.F., 1986, Airborne estimation of sea turbidity parameters in an airborne laser hydrographic system. Applied Optics, 25, 2080-2088.

Bristow, M.P.F., Bundy, D., Edmonds, C.M., Ponto, P.E., Frey, B.E., and Smal, L.F., 1985, Airborne laser fluorosensor survey of the Columbia and Snake rivers: simultaneous measurements of chlorophyll, dissolved organics and optical attenuation. International Journal of Remote Sensing, 6, 1707-1734).

Camagni, P., Colombo, A., Koechler, C., Omenetto, N., Qi, P., and Rossi, G., 1991, Fluorescence response of mineral oils: spectral yield vs. absorption and decay time. Applied Optics, 30, 26-35.

Cecchi, G., Pantani, L., Breschi, B., Tirelli, T., and Valmori, G., 1992, Flidar: A multipurpose fluorosensor-spectrometer. EARSeL Advances in Remote Sensing, 1, 72-78.

Determann, S., Reuter, R., Wagner, P., and Willkomm, R., 1994, Fluorescent matter in the eastern Atlantic Ocean. Part 1: method of measurement and near-surface distribution. Deep-Sea Research, in press.

Diebel-Langohr, D., Hengstermann, T., and Reuter, R., 1986, Water depth resolved determination of hydrographic parameters from airborne lidar measurements. In: Marine Interfaces Ecohydrodynamics, J.C.J. Nihoul (editor), (Amsterdam: Elsevier), pp. 591-602.

Diebel, D., 1987a, Tiefenaufgelöste Laserfernerkundung geschichteter Strukturen im Meer unter Verwendung von Gelbstoff als Tracersubstanz. PhD Thesis, University of Oldenburg, May 1987, 159 pp.

Diebel, D., Hengstermann, T., and Reuter, R., 1987b, Classification of oil types with time-resolved fluorescence detection: a computer model study. In: Remote Sensing of Pollution of the Sea, R. Reuter and R.H. Gillot (editors), (Oldenburg: BIS der Universitt; Ispra: Joint Research Centre), S.P.I. 87.46, pp. 266-280.

Dudelzak, A., Babichenko, S.M., Poryvkina, L.V., and Saar, K., 1991, Total luminescent spectroscopy for remote laser diagnostics of natural water conditions. Applied Optics, 30, 453-458.

Gordon. H.R., 1982, Interpretation of airborne oceanic lidar: effects of multiple scattering. Applied Optics, 21, 2996-3000.

Hoge, F.E., and Swift, R.N., 1982, Delineation of estuarine fronts in the German Bight using airborne laser-induced water Raman backscatter and fluorescence of water column constituents. International Journal of Remote Sensing, 3, 475-495.

Hoge, F.E., and Swift, R.N., 1983, Airborne detection of oceanic turbidity cell structure using depth-resolved laser-induced water Raman backscatter. Applied Optics, 22, 3778-3786.

Hoge, F.E., Wright, C.W., Krabill, W.B., Buntzen, R.R., Gilbert, G.D., Swift, R.N., Yungel, J.K., and Berry, R.E., 1988, Airborne lidar detection of subsurface oceanic scattering layers. Applied Optics, 27, 3969-3977.

Leonard, D.A., Caputo, B., and Hoge, F.E., 1979, Remote sensing of subsurface water temperature by Raman backscattering. Applied Optics, 18, 1732-1745.

Measures, R.M., 1984, Laser Remote Sensing. Fundamentals and Applications. (New York: Wiley), 510 pp.

Ohm, K., and Willkomm, R., 1994, Collecting performance of a lidar telescope at short distances. EARSeL Advances in Remote Sensing, paper included in this volume.

Phillips, D.M., 1981, Effect of water turbidity on laser depth sounding performance. In: Proceedings of the Fourth Laser Hydrography Symposium, 30 Sept.-3 Oct. 1980, Document AR-002-576, Report ERL-193-SD, M.F. Penny and D.M. Phillips (editors), Adelaide, Australia

Poole, L.R., and Esaias, W.E., 1982, Water Raman normalization of airborne laser fluorosensor measurements: A computer model study. Applied Optics, 21, 3756-3761.

Punjabi, A., and Venable, D.D., 1986. Effects of multiple scattering on time- and depth-resolved signals in airborne lidar systems. International Journal of Remote Sensing, 7, 615-626.

Reuter, R., Diebel, D., and Hengstermann, R., 1993, Oceanographic laser remote sensing: measurements of hydrographic fronts in the German Bight and in the northern Adriatic Sea. International Journal of Remote Sensing, 14, 823-848.

Schmitz-Peiffer, A., and GRAaL, H., 1990a, Remote Sensing of coastal waters by airborne lidar and satellite radiometer. Part 1: a model study. International Journal of Remote Sensing, 11, 2163-2184.

Schmitz-Peiffer, A., Viehoff, T., and Graβl, H., 1990b, Remote Sensing of coastal waters by airborne lidar and satellite radiometer. Part 2: Measurements. International Journal of Remote Sensing, 11, 2185-2204.

Tatischeff, I., and Klein, R., 1976, Fluorescence quantum yield of the aromatic amino acids as a function of excitation wavelength. In: Excited States of Biological Molecules, J.B. Birks (editor), (London: Wiley), pp. 375-387.

Venable, D.D., Punjabi, A.R., and Poole, L.R., 1984, Sensitivity of airborne fluorosensor measurements to linear vertical gradients in chlorophyll concentration. Applied Optics, 23, 971-972.

Verdebout, J., and Koechler, C., 1992, Nanosecond time resolution: Technical, implementation and usefulness. EARSeL Advances in Remote Sensing, 1, 61-71.